Role of bending mode in generation of angular momentum of fission fragments

T. M. Shneidman,[1,2] G. G. Adamian,[1,2,3] N. V. Antonenko,[1,2] S. P. Ivanova,[1,2] R. V. Jolos,[1,2] and W. Scheid[1]
[1]*Institut für Theoretische Physik der Justus-Liebig-Universität, D-35392 Giessen, Germany*
[2]*Joint Institute for Nuclear Research, RU-141980 Dubna, Russia*
[3]*Institute of Nuclear Physics, Tashkent 702132, Uzbekistan*
(Received 5 March 2001; revised manuscript received 4 March 2002; published 23 May 2002)

Based on the dinuclear system concept, the role of bending vibrations in creation of the angular momentum of the primary fission fragments is investigated. For ^{252}Cf spontaneous fission, the angular momenta of the fragments are calculated as a function of the neutron multiplicity and compared with available experimental data.

DOI: 10.1103/PhysRevC.65.064302 PACS number(s): 24.75.+i, 21.60.Gx

I. INTRODUCTION

The phenomenon of nuclear molecular resonances, whose description requires one to consider the relative motion of two nuclei, has been known for a long time from the study of reactions with certain light nuclei [1–3]. For heavy nuclei, the experimental facts indicate the formation of a dinuclear system (DNS) with quite a long lifetime (a few units of 10^{-21} s) that was detected in deep inelastic reactions with heavy ions at energies lower than 15 MeV/nucleon [4,5]. When the DNS evolves in mass (charge) asymmetry, its decay in a relative coordinate R between the centers of nuclei determines the charge and mass distribution of reaction products [4,5]. An evolution of a DNS to a compound nucleus by the transfer of nucleons from the light nucleus to the heavy one has been considered in Refs. [6,7].

Just before the scission, when the neck radius is small, the fissioning system can be treated as a system of two aligned, deformed nuclei separated by a constant distance between their tips [8–20]. Thermal equilibrium is usually assumed in a DNS. In order to describe the dependence of experimental data on the total kinetic energy (TKE) of fission fragments, we consider the pole-pole configuration of the DNS. The main observables, such as the distributions of mass, charge, and kinetic energy, in the fission of a wide range of nuclei from Po to Fm are reproduced well within scission-point models [12]. Fragmentation theory [3] treats fission as a quantum-mechanical process in the relative distance and mass asymmetry coordinates and qualitatively explains the general features of fission mass distributions.

The experimental data show that the difference of the potential energy between the saddle and scission configurations (several tens of MeV) is not completely transformed into the total kinetic energy of relative motion of fission fragments, but other collective or intrinsic degrees of freedom absorb the rest of the energy. Different types of collective angular vibrations, such as wriggling, bending, tilting, and twisting, are possible in the excited prescission DNS [5,8,21–24]. These collective modes do not contribute to the kinetic energy of fragments after the decay of the DNS. Angular vibrations can generate the rotational energy and angular momenta of the fragments of binary and ternary fissions [25]. The generation of angular momenta of fission fragments was treated by several authors many years ago [8,9,11]. They showed that the bending vibrations are the main source by which the fragments gain angular momentum at scission point. A recent experimental study of spontaneous fission of ^{252}Cf with the Gammasphere detector provides information about the average angular momentum of fission fragments [16,26]. While the fissioning nucleus has initially zero spin, the primary fission fragments have angular momenta of about $(2-8)\hbar$ [26]. These data result from the study of γ transitions between the levels of ground-state rotational bands of the fragments.

The main purpose of our paper is the explanation and description of the dependence of angular momenta of fission fragments of ^{252}Cf on the number of emitted neutrons. We will show that the temperature in our model is not a free parameter and corresponds to the excitation energy of the internal degrees of freedom. The production of angular momentum in the fission fragments and the method of calculation of the DNS potential and excitation energies are described in Secs. II and III, respectively. The angular momenta of fission fragments are calculated in Sec. IV as a function of the number of postscission neutrons, under the assumption of bending angular vibrations at the scission point by which the fragments gain angular momentum. For ^{252}Cf spontaneous fission, the calculated results are compared with the experimental data. A summary is given in Sec. V. The method of calculation of the potential energy of bending mode is presented in the Appendix.

II. BENDING VIBRATIONS

At the scission point, a fissioning system can be approximately considered as a DNS whose intrinsic degrees of freedom are in thermal equilibrium. However, a shape of the DNS is not equilibrated. In this paper, we assume that the angular momenta of fission fragments are generated by small bending vibrations of DNS nuclei around the pole-pole orientation. A similar assumption was earlier done in Refs. [8,9,11,16,20]. In the bending mode, the rolling of nuclear surfaces occurs. The slide of nuclear surfaces in the wriggling mode is assumed to be suppressed by friction [21,27] and larger stiffness of the potential. Since the fissioning nucleus has initially zero spin, the wriggling mode would need larger rotational energy because of larger orbital momentum compensating the spins of the fragments. Therefore,

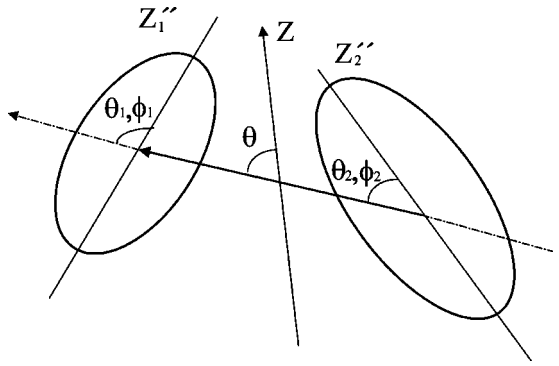

FIG. 1. Schematic picture and definitions of various coordinates of the DNS configuration.

the wriggling mode is energetically unfavorable.

The Hamiltonian describing collective modes of a DNS (nuclear molecule) was analyzed in [22] where suitable coordinates were introduced, and an expression for the kinetic energy operator was derived. The procedure of quantization of the classical Hamiltonian is described in Ref. [22]. Below we consider the case of axially deformed DNS nuclei and also eliminate β and γ vibrations of the clusters and oscillations of an intercluster distance around the equilibrium value from the consideration. The frequency of oscillations in R is at least three times as large as those for angular vibrations. The equilibrium distance $R=R_m \approx R_1[1-\beta_1^2/(4\pi)+\sqrt{5/(4\pi)}\beta_1]+R_2[1-\beta_2^2/(4\pi)+\sqrt{5/(4\pi)}\beta_2]+0.5$ fm between the centers of nuclei corresponds to the minimum of the nucleus-nucleus potential which is a sum of nuclear and Coulomb potentials U_N and U_C [28]:

$$U(R,\beta_i,\Omega_i)=U_C(R,\beta_i,\Omega_i)+U_N(R,\beta_i,\Omega_i). \tag{1}$$

Here, the angles $\Omega_i=(\theta_i,\phi_i)$ $(i=1,2)$ specify the orientation of the intrinsic coordinate system of an ith nucleus with respect to the molecular frame whose z axis goes through the centers of nuclei forming DNS, β_i are deformation parameters.

The coordinates used to describe the motion of clusters forming DNS are shown in Fig. 1. The center of this coordinate frame lies at the DNS center of mass. The angle θ is the angle of rotation of DNS as a whole. The angles θ_1 and θ_2 specify the orientation of the cluster with respect to the axis connecting the centers of mass of clusters. The angles ϕ_1 and ϕ_2 specify their azimuthal orientation. The angles θ_1 and θ_2 are related via the condition that clusters touch each other at the poles [22]. If this condition is not fulfilled, the potential energy increases considerably. Under this condition

$$\frac{\tilde{R}_2}{\tilde{R}_1}\approx\frac{\sin|\pi-\theta_1|}{\sin|\theta_2|}, \tag{2}$$

where $\tilde{R}_i=R_i[1-\beta_i^2/(4\pi)+\sqrt{5/(4\pi)}\beta_i]$ and $R_i=r_0A_i^{1/3}$ are the radii along the symmetry axis of clusters having prolate deformation and their spherical radii, respectively. If only small values of $(\pi-\theta_1)$ and θ_2 are allowed, then

$$\tilde{R}_1(\pi-\theta_1)=-\tilde{R}_2\theta_2. \tag{3}$$

Using the constraint (3), the problem under consideration is simplified to the one-dimensional Shrödinger equation with analytical solution (see below). For almost symmetric DNS, we checked that the approximation (3) is suitable. Thus, the bending degree of freedom is given by

$$\epsilon=\pi-\theta_1. \tag{4}$$

Under the assumption formulated above, the model Hamiltonian describing the rotation of the DNS as a whole and small bending angular vibrations can be written as [22]

$$H=T_{\rm rot}+T_\epsilon+U_\epsilon, \tag{5}$$

where $T_{\rm rot}$ describes the rotation of DNS as a whole, T_ϵ is the kinetic energy of bending motion

$$T_\epsilon=-\frac{\hbar^2}{2J_\epsilon}\frac{1}{\epsilon}\frac{d}{d\epsilon}\left(\epsilon\frac{d}{d\epsilon}\right), \tag{6}$$

$$J_\epsilon=J_1+(\tilde{R}_1/\tilde{R}_2)^2J_2. \tag{7}$$

Here, $J_{1,2}$ are moments of inertia of clusters forming DNS, U_ϵ is the potential energy of bending motion, the volume element is $dV=\epsilon d\epsilon$.

Using the condition that the total angular momentum of a decaying system is zero and constraint (3), one can express the angle θ through ϵ

$$\theta=\frac{J_1\tilde{R}_2-J_2\tilde{R}_1}{\tilde{R}_2(\mu R_m^2+J_1+J_2)}\epsilon. \tag{8}$$

It is seen from Eq. (8) that, for a nearly symmetric DNS, $\theta\approx 0$ and the role of $T_{\rm rot}$ in Eq. (5) is negligible.

The potential energy was considered in Ref. [22] only schematically. The aim of the present paper is to apply the potential energy calculated by us in previous publications [28] for calculations of angular momenta of fission fragments. It was applied for analysis of the experimental data on fusion and deep inelastic collisions. The potential energy is calculated in the Appendix taking Eq. (3) into account. We neglect, as was mentioned above, the oscillations of the intercluster distance. Due to the axial symmetry of the DNS nuclei, the potential energy does not depend on the azimuthal vibrations. Then for small deviations of the ratio of angles θ_1 and θ_2 from Eq. (3), the potential energy of bending vibrations takes the form

$$U_\epsilon=\frac{1}{2}C_{11}(\pi-\theta_1)^2+C_{12}(\pi-\theta_1)\theta_2+\frac{1}{2}C_{22}\theta_2^2. \tag{9}$$

The stiffness coefficients C_{11}, C_{12}, and C_{22} are given in the Appendix.

Using the condition (3) and notation (4), we get from Eq. (9)

$$U_\epsilon=\frac{1}{2}C_\epsilon\epsilon^2, \tag{10}$$

where

$$C_\epsilon = C_{11} - 2(\tilde{R}_1/\tilde{R}_2)C_{12} + (\tilde{R}_1/\tilde{R}_2)^2 C_{22}. \quad (11)$$

Thus, we get the following Schrödinger equation for the bending vibrations:

$$-\frac{\hbar^2}{2J_\epsilon}\frac{1}{\epsilon}\frac{d}{d\epsilon}\epsilon\frac{d}{d\epsilon}\psi_n + \frac{1}{2}C_\epsilon\epsilon^2\psi_n = E_n\psi_n. \quad (12)$$

The solutions of Eq. (12) are

$$\psi_n(\epsilon) = N_0 L_n(J_\epsilon\omega_\epsilon\epsilon^2/\hbar)\exp[-J_\epsilon\omega_\epsilon\epsilon^2/(2\hbar)],$$

$$E_n = \hbar\omega_\epsilon(2n+1), \quad n = 0,1,2,\ldots, \quad (13)$$

where $\omega_\epsilon = \sqrt{C_\epsilon/J_\epsilon}$; $N_0 = \sqrt{2J_\epsilon\omega_\epsilon/\hbar}$ and $L_n(x)$ are the normalization coefficient and the Laguerre polynomial [29], respectively.

In order to estimate the angular momentum of the bending mode, we expand $\psi_n = \sqrt{2\pi}\Sigma_L b_n^L Y_{L0}(\theta, \phi = 0)$ into spherical harmonics. With the expansion coefficients b_n^L [9]

$$|b_n^L|^2 = (2L+1)\gamma_0^2\{L_n[(L+0.5)^2\gamma_0^2]\}^2\exp[-(L+0.5)^2\gamma_0^2],$$

we determine the average value of angular momentum $\langle L\rangle_n$ in the state ψ_n as follows:

$$\langle L\rangle_n = \sum_L L|b_n^L|^2. \quad (14)$$

Here, $\gamma_0^2 = \hbar\omega_\epsilon/C_\epsilon = \hbar/\sqrt{J_\epsilon C_\epsilon}$. If the DNS is in thermal equilibrium with an excitation energy E^* (the corresponding temperature is $\Theta = \sqrt{E^*/a}$, $a = A/12$ MeV^{-1}), the average angular momentum $\langle L\rangle$ is calculated as

$$\langle L\rangle = \sum_n \langle L\rangle_n P_n \Big/ \sum_n P_n, \quad (15)$$

where $P_n = \exp[-E_n/\Theta]$ is the Boltzmann-like occupation probability of the nth bending state. The applicability of the Boltzmann factor was demonstrated many times for the description of the mass, charge, angular, and kinetic energy distributions of fission fragments in the scission-point models. The exact population probability of a given bending state is well approximated by the Boltzmann factor. Since the potential for the bending vibrations has a finite depth, in addition to the smallness of P_n, the maximal value of n in Eq. (15) should be restricted by the capacity of this potential to hold a certain number of bound states ψ_n. However, for the temperatures considered, this restriction of n does not affect results. Note that the maximal value of n is discussed only in connection with the second fission mode of ^{252}Cf.

III. COMPARISON WITH OTHER APPROACHES

The multidimensional collective Hamiltonian of the dinuclear systems was treated in Refs. [8,9,11,22–24]. The states related to the bending and wriggling modes are the solutions of the Schrödinger equation for two coupled two-dimensional rotators [11]. Since the angles θ_2 and $\pi - \theta_1$ are small, the Schrödinger equation is transformed into the form of two coupled two-dimensional harmonic oscillators. Following Ref. [22], we simplified the problem to the one-dimensional equation (11) using the constraint (3). The relation (3) comes in a natural way because in the classical bending motion the DNS nuclei touch each other. Among all collective modes contributing to the angular momentum of fragments with Eq. (3) we select the one with maximal contribution because the potential energy significantly increases when the angles $\pi - \theta_1$ and θ_2 change independently and the touching condition (3) is not fulfilled. For almost symmetric DNS, we obtained that the solutions of one- and two-dimensional Schrödinger equations gave practically the same results. So, the condition (3) is correct for the problem under consideration.

As in the present paper, the spectrum of bending vibrations is defined in Refs. [9,15,22] by $\hbar\omega_\epsilon(2n+1)$. Since in Ref. [15] the moment of inertia J_ϵ is calculated in irrotational limit, the obtained values of $\hbar\omega_\epsilon$ are a few times larger than in our treatment. The generation of angular momentum of fission fragments is not considered in Ref. [15].

The angular momenta of fragments in the neutronless spontaneous fission of ^{252}Cf have been treated in Ref. [20], where the two coupled two-dimensional rotators are erroneously changed by the two coupled one-dimensional oscillators, for which these authors, of course, obtained an analytical expression for the average squared angular momentum of fragments. This leads to the spectra of bending and wriggling modes given simply by the sum of two one-dimensional harmonic oscillator spectra. Indeed, the two coupled rotators cannot be transformed by the two coupled one-dimensional harmonic oscillators (or by the one-dimensional harmonic oscillator when the angles θ_1 and θ_2 are connected by some constraint). The bending and wriggling modes are not harmonic oscillator vibrations but the angular vibrations. The metric tensor for the bending motion is different from that for the harmonic oscillator motion (see the previous section).

The approach different from the activation of spins through collective degrees of freedom has been claimed in Ref. [18]. However, we think that this approach is not much different from the approaches based on the collective model. The experimentally observed γ quanta indicate the collective rotation of fission fragments. The collective motion remains collective in spite of different descriptions. In our opinion, if the so-called intrinsic wave function in Ref. [18] was pure intrinsic, the formalism of Ref. [18] would lead to spurious angular momenta and spurious electromagnetic transitions for the separated deformed fragments. The expectation value of the squared angular momentum $\langle L^2\rangle$ in Ref. [18] can be associated with the collective rotation if the probability amplitudes a_L of the distribution of different angular momentum L states in each deformed fragment are connected with the zero-point fluctuations of orientation angles (based on the minimal uncertainty relation) of the fission fragments at scission. Indeed, if one takes $L(L+1)$ and $\langle J_i\rangle_{\rm int}$ instead $(L+0.5)^2$ and γ_0^{-2}, respectively, the expression for a_L in Ref. [18] is the same as the one for b_0^L in present paper. Since the deformed fragments are approximated as the two nonin-

teracting rotors which are coupled to zero total spin, the analytical expression for $\langle L^2 \rangle$ in Ref. [18] seems to be a crude approximation. In the present paper the interaction between fragments is not disregarded and the motion of each fragment at scission is the motion of a constrained rotor.

IV. EXCITATION ENERGY OF DNS AND TKE OF FISSION FRAGMENTS

In order to calculate the average angular momentum of fission fragments by Eq. (15), we should determine the excitation energy of DNS before its decay. The dependence of the average angular momentum of primary fission fragments on the number of evaporated neutrons is extracted from the experiment [16,26]. For comparison with the theory, we have to establish a relation between the DNS excitation energy E^* and the number of evaporated neutrons after the DNS decay.

With the assumption that the prescission kinetic energy of fission fragments is very small [12], the total energy $E_{\rm total}$ of DNS is estimated as

$$E_{\rm total}=E^*+E_n+U_{\rm int}+B_1^{\rm def}+B_2^{\rm def}, \tag{16}$$

where E_n, $U_{\rm int}=U(R_m,\beta_i,\Omega_i)$ [see Eq. (1)], and $B_i^{\rm def}$ ($i=1,2$) are the energy of bending vibrations, the energy of interaction of DNS nuclei, and the binding energies of the DNS deformed nuclei, respectively. Note that $B_i^{\rm def}$ differs from the experimental binding energy B_i of separated nuclei in their ground state [30]. Since the energies E_n of low-lying bending states, which give the main contributions to angular momentum, does not exceed a few MeV and are comparable with an accuracy of calculation of $U_{\rm int}$, we can neglect E_n in Eq. (16). Indeed, this additional term in Eq. (16) does not visibly change the calculated temperature. After the decay, the total energy $E_{\rm total}$ of the system can be estimated as follows:

$$E_{\rm total}=E_\nu+{\rm TKE}+B_1+B_2, \tag{17}$$

where E_ν is the energy taken by ν evaporated neutrons. Assuming that the interaction energy $U_{\rm int}$ of DNS nuclei is approximately equal to the TKE and using the equality of the two previous expressions, we define the excitation energy E^* as

$$E^*=E_\nu-\Delta B_1-\Delta B_2=E_\nu-(B_1^{\rm def}-B_1)-(B_2^{\rm def}-B_2). \tag{18}$$

If the deformation energy $\Delta B_1+\Delta B_2$ required to deform the DNS nuclei from their ground states is small, we obtain

$$E^*\approx E_\nu=\sum_{m=1}^{\nu}(S_m+2\Theta_m), \tag{19}$$

where the average kinetic energy of an mth evaporated neutron is equal to twice the temperature Θ_m of fragments. The separation energies S_m of the mth neutron of the first or second fragment are taken from Ref. [30]. Since the number of evaporated neutrons from each primary fission fragment is available [16,26], the value of E_ν is easily calculated. In the DNS, we deal with two distinct nuclei. Therefore, the decay of DNS is not the same as the scission in the traditional description of fission, and the comparison of prescission excitation energy obtained in this description with E^* cannot be done. In this paper, we assume that the fissioning nucleus after the scission lives for some time as the DNS.

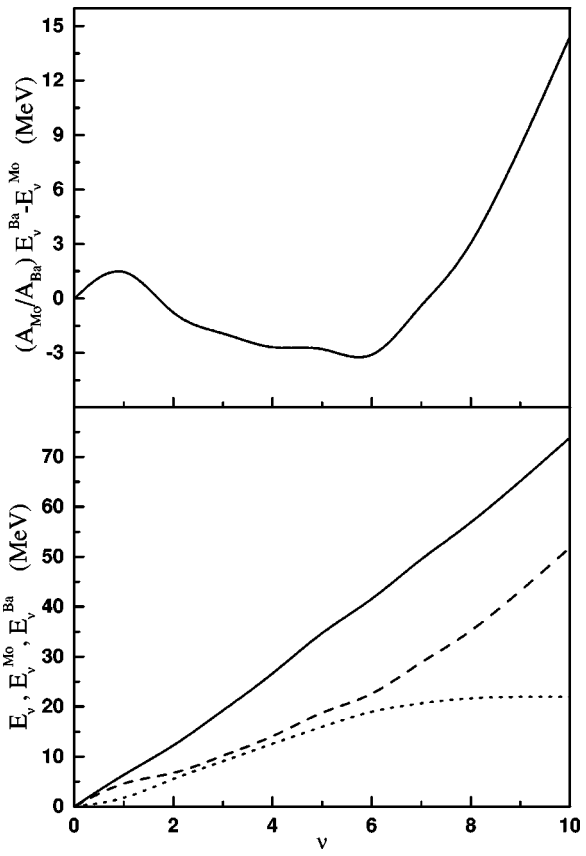

FIG. 2. The values of $(A_{\rm Mo}/A_{\rm Ba})E_\nu^{\rm Ba}-E_\nu^{\rm Mo}$ (upper figure), $E_\nu^{\rm Ba}$, $E_\nu^{\rm Mo}$, and E_ν (lower figure: long-dashed, short-dashed, and solid curves, respectively) as a function of the number of evaporated neutrons ν from both nuclei are presented for primary fission fragments ^{104}Mo+^{148}Ba of ^{252}Cf. The excitation energies of the primary fission fragments $E_\nu^{\rm Ba}$ and $E_\nu^{\rm Mo}$ ($E_\nu=E_\nu^{\rm Ba}+E_\nu^{\rm Mo}$) are taken from experimental data [26].

If we consider the decay of ^{252}Cf into the Mo-Ba fragmentation, the value of $(A_{\rm Mo})/(A_{\rm Ba})E_\nu^{\rm Ba}-E_\nu^{\rm Mo}$ characterizes the distribution of the excitation energy $E_\nu=E_\nu^{\rm Ba}+E_\nu^{\rm Mo}$ between primary fission fragments. Using the experimental data [26], we can calculate the dependence of $(A_{\rm Mo})/(A_{\rm Ba})E_\nu^{\rm Ba}-E_\nu^{\rm Mo}$ on ν. In Fig. 2, one can see that up to $\nu=5$ the excitation energy is approximately distributed proportionally to the masses of fragments. This indicates the validity of Eq. (19). For $\nu>5$, the difference between E^* and E_ν becomes large, and we should take the value of $\Delta B_1+\Delta B_2$ into consideration. From Fig. 2, we can see that the deformation energy is larger in Ba than in Mo.

V. RESULTS OF CALCULATIONS

A. Different fission modes

Calculating the nucleus-nucleus interaction is calculated with Eq. (1) and the deformation energy with the two-center

shell model [3,31], we found that the equilibrium deformations of the DNS nuclei deviate from their values in the ground states due to the polarization effects. The quadrupole deformations of ^{104}Mo and ^{148}Ba are $\beta_1=0.50$ and $\beta_2=0.40$, respectively. The interaction of the DNS nuclei with found deformations corresponds to the average total kinetic energy $\langle \mathrm{TKE}\rangle = 189\pm 1$ MeV for the first (standard) fission mode of ^{252}Cf leading to the Mo-Ba fragmentation. For ^{104}Mo and ^{148}Ba, we obtained $\Delta B_1=0.4$ MeV at $\beta=0.5$ and $\Delta B_2=2.2$ MeV at $\beta=0.4$, respectively. These ΔB_i values are more than two times smaller than those obtained in Ref. [19] with constrained HF+BCS calculations using the Skyrme interaction SIII. One of the imposed constraints in Ref. [19] is that the excitation energy is accounted only by the deformation energy. However, the difference in ΔB_i is within uncertainty 5 MeV [19] for such calculations. In order to avoid the uncertainty created by the choice of the parameters of microscopic calculations, we use the experimental values of nuclear mass parameter and stiffness with respect to the deformation for finding ΔB_i from

$$\Delta B_i = D_{\beta i}\omega_{\beta i}^2(\beta_i-\beta_{i0})^2, \tag{20}$$

where $D_{\beta i}$ and $\omega_{\beta i}$ are the mass parameter and the frequency of the β vibration in the ith nucleus, respectively. The quadrupole deformations of ^{104}Mo and ^{148}Ba extracted from the reduced $E2$ transition probabilities from the ground state to the first 2^+ state are $\beta_{10}=0.35$ and $\beta_{20}=0.22$, respectively [32]. Using the experimental data for $D_{\beta i}$ and $\omega_{\beta i}$ [32], one can show that the values of ΔB_i do not exceed 1.0 MeV for considered fragmentations of ^{252}Cf. Since the excitation energy is shared between the fragments proportionally to their masses when the number of emitted neutrons does not exceed 5 units (Fig. 2), the deformation energy is expected to be small as in Eq. (20) and can be neglected in Eq. (18). The fact that the deformation energy is small is supported by microscopic calculations giving an energy difference of a few MeV between the superdeformed and ground states even at zero angular momentum [33,34]. Since ΔB_i are quite small, the difference Q-TKE mainly corresponds to the excitation energy of internal degrees of freedom of the DNS for $\nu<5$ for the case of Mo+Ba splitting. This means that the DNS is heated before the scission, and we can use the statistical treatment to find the average angular momentum of each fragment. In the calculations, we consider bending vibrations in the DNS with $\Theta<1$ MeV that corresponds to excitation energies less than 30 MeV. The coupling between the internal degrees of freedom and the relative motion determines the distribution of TKE. To explain the TKE for the fission events with $\nu>5$, larger deformations of DNS nuclei should be taken into account for which the values of ΔB_i are not negligible. Note that for other splitting ΔB_i could be sufficient starting with smaller ν.

The second fission mode in the fragmentation of ^{252}Cf into Mo and Ba corresponds to unusually small $\langle \mathrm{TKE}\rangle = 153\pm 3$ MeV and a large number of emitted neutrons. In this mode, the fragments are highly excited and evaporate more than seven neutrons. Due to the experimental difficulties of resolving nearly identical transition energies in ^{104,108}Mo, there is discussion [35] about the existence of the second mode of highly excited fragment in the Mo-Ba split. A low TKE means enormously elongated nuclei in the decaying DNS. Since the attractive nuclear part of nucleus-nucleus potential decreases with increasing deformation of the DNS nuclei, the formation of the DNS consisting of highly deformed nuclei is strongly restricted. This could be a reason for very small probability of a realization of the second mode, if it exists.

The large deformations of fragments in the second fission mode can be described, for example, by the following cluster states of the nuclei $^{148}\mathrm{Ba}\rightarrow {}^{74}\mathrm{Ni}+{}^{74}\mathrm{Ni}$ and $^{104}\mathrm{Mo}\rightarrow {}^{50}\mathrm{Ca}+{}^{54}\mathrm{Ti}$. The deformation energies are equal to 20 and 15 MeV ($\Delta B=35$ MeV) for such cluster configurations and are close to those for hyperdeformed nuclei [36]. The linear chain $({}^{74}\mathrm{Ni}+{}^{74}\mathrm{Ni})+({}^{50}\mathrm{Ca}+{}^{54}\mathrm{Ti})$ with the deformations of nuclei taken from [32] reproduces the $\langle \mathrm{TKE}\rangle$ for the second fission mode. The excitation energy E^* of the system near scission is about 30 MeV. After the scission, the systems $^{74}\mathrm{Ni}+{}^{74}\mathrm{Ni}$ and $^{50}\mathrm{Ca}+{}^{54}\mathrm{Ti}$ are transformed into ^{148}Ba and ^{104}Mo, respectively, with the transition of deformation energies into intrinsic excitations. The system $^{102}\mathrm{Zr}+{}^{4}\mathrm{He}+{}^{4}\mathrm{He}+{}^{142}\mathrm{Xe}$ which supplies the experimental TKE could also be used for the second fission mode. The calculation of the angular momenta of the fragments can be done by assuming a rigid coupling between the α particles and heavy nuclei. This approximation can be applied because the bending frequency of a system consisting of an α particle and a heavy nucleus is much larger than that for the whole system. The analysis of similar cluster configurations allows us to expect the second fission mode with very low $\langle \mathrm{TKE}\rangle$ for the charge splittings Zr-Ce and Ru-Xe. Further experiments will give the answer whether our assumption is correct. In spite of small probability of the formation of three- and four-cluster configurations in fission, they cannot be disregarded in the analysis of the second mode, if one exists. There is experimental evidence for the cluster interpretation of prescission configurations in fission [14]. The bending modes for the three- and four-cluster configurations in fission can be considered analogously to the binary configurations [25].

B. Angular momentum generating by bending mode

The potential energy of the DNS as a function of the relative distance R for the fission $^{252}\mathrm{Cf}\rightarrow {}^{104}\mathrm{Mo}+{}^{148}\mathrm{Ba}$ is shown in the upper part of Fig. 3. It is seen that the DNS pole-pole configuration has a minimal energy. The minimum of the pocket is located at the distance R_m. This minimum moves to smaller values of the relative distance with increasing angles $\tilde{\theta}_i$ ($\tilde{\theta}_1=\pi-\theta_1, \tilde{\theta}_2=\theta_2$). In the lower part of Fig. 3, the dependence of the potential energy on the angles $\tilde{\theta}_i$ is shown in the following two limits. (1) The relative distance corresponds to the minimum of the potential energy at all values of angles (adiabatic limit). (2) The relative distance does not change [$R=R_m(\tilde{\theta}_i=0)=\mathrm{const}$] with angles (diabatic limit). For $|\tilde{\theta}_1|<0.5$, the potentials in these two limits are very similar. It is seen that the oscillator approximation is quite good for the description of the angular dependence of

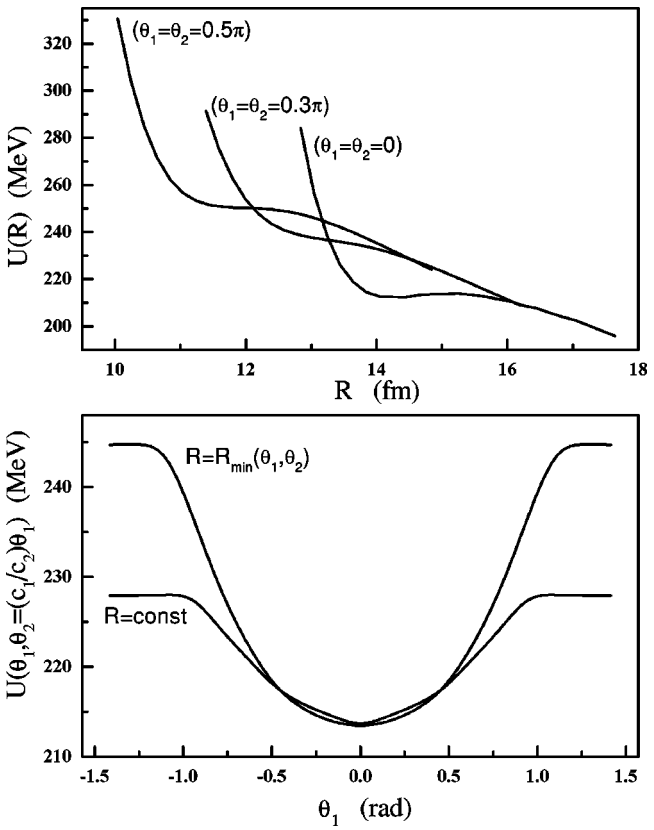

FIG. 3. Upper part: Dependence of the DNS potential energy on the relative distance R between the centers of fragments for the fission of $^{252}\mathrm{Cf}\rightarrow{}^{104}\mathrm{Mo}+{}^{148}\mathrm{Ba}$. Calculations are done for different orientations of DNS nuclei with $\beta_1(^{104}\mathrm{Mo})=0.35$ and $\beta_2(^{148}\mathrm{Ba})=0.22$. Lower part: Calculated potential energy U of the DNS as a function of the angles $\tilde{\theta}_i$ in the two limits. (1) $R=R_m$ (adiabatic limit) and (2) $R=R_m(\tilde{\theta}_i=0)$ (diabatic limit). The relation $\tilde{\theta}_2=(\tilde{R}_1/\tilde{R}_2)\tilde{\theta}_1$ is used in the calculations.

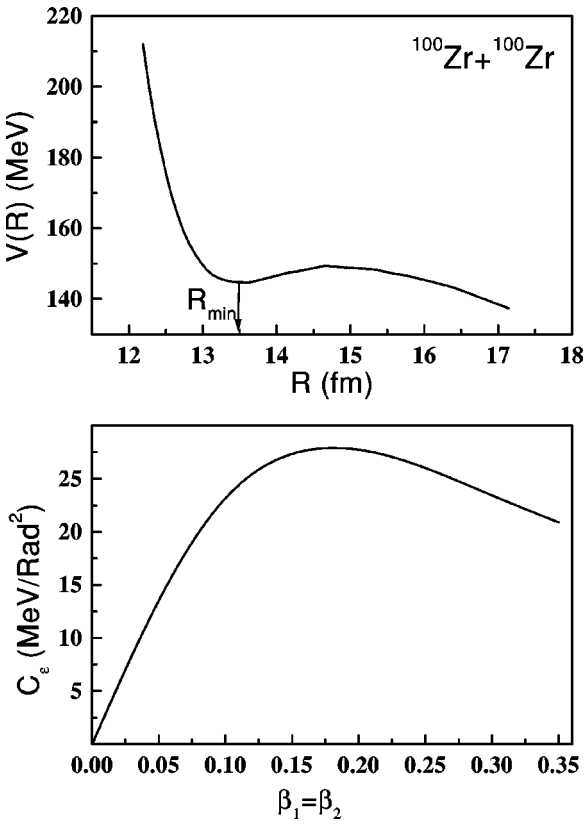

FIG. 4. Upper part: The DNS potential as a function of the relative distance R between the centers of fragments for the symmetric system $^{100}\mathrm{Zr}+{}^{100}\mathrm{Zr}$ with $\beta_1=\beta_2=0.3$. Lower part: The calculated stiffness parameter C_ϵ of the bending mode in DNS as a function of the quadrupole deformation parameters $\beta_1=\beta_2$ for the symmetric system $^{100}\mathrm{Zr}+{}^{100}\mathrm{Zr}$.

the potential energy, if the amplitude does not exceed 0.5 rad. In Fig. 4, we present the dependence of the stiffness parameter of the bending mode on deformation parameters for the $^{100}\mathrm{Zr}+{}^{100}\mathrm{Zr}$ system. The value of stiffness strongly increases with the deformation parameters $\beta_1=\beta_2$ from zero and reaches a nearly constant value at $0.12<\beta_i<0.25$. For $\beta_i>0.25$, the stiffness decreases slowly. Thus, for $\beta_i>0.12$ the calculated results seem to be weakly sensitive to the value of the deformation parameters, because the stiffness of the potential depends weakly on β_i.

In order to estimate the mean angular momenta of the fission fragments by Eq. (15), we calculated the spectrum of the bending mode for various fragmentations of the $^{252}\mathrm{Cf}$ nucleus. The influence of the fragment deformations β_i and moments of inertia J_i on the excitation of bending states is demonstrated in Table I. In this calculation, we use the experimental moments of inertia J_i of DNS nuclei which are obtained from the measured values of the energies $E_{2^+\rightarrow 0^+}$ of the $2^+\rightarrow 0^+$ rotational transitions $J_i=3/E_{2^+\rightarrow 0^+}$ ($\hbar^2$/MeV) [32]. When both fragments are well deformed, the energy E_1 of the first excited state [$n=1$ in Eq. (13)] of the bending mode is about (1.5–2.0) MeV. If one of the fragments is almost spherical, the value of E_1 is about (3.0–6.0) MeV.

The experimental [16] and calculated angular momenta of fission fragments as a function of the total number of evaporated neutrons ν are presented in Figs. 5 and 6 for the fragmentations Mo+Ba and Zr+Ce of $^{252}\mathrm{Cf}$. The value of E^* is estimated by formula (19) for the standard fission mode assuming that ΔB_i is small. Since the potential for the bending oscillation in this fission mode is deep enough and contains quite a large number of states, the calculated values of $\langle L\rangle$ practically do not depend on the upper limit of sums in Eq. (15). The calculations of angular momentum for the standard fission mode were performed by using the experimental and rigid body moments of inertia of the nuclei. The experimental moment of inertia of a nucleus is smaller than the rigid body one. However, for a system of two interacting nuclei in the field of each other, realistic moments of inertia of nuclei must take values between two considered limits. For example, the measured moments of inertia for superdeformed and hyperdeformed states are about 85% of the rigid body value [33,34,36]. A possibility to consider highly deformed states in heavy nuclei as DNS configurations was demonstrated in Ref. [36]. Indeed, the corresponding DNS have the same quadrupole moments and moments of inertia as those measured for the superdeformed states and for the hy-

TABLE I. Calculated values of the frequency $\hbar\omega_\epsilon$ and the moment of inertia J_ϵ of the bending mode for even-even fragmentations of ^{252}Cf. Θ is the temperature for the dinuclear configuration with given quadrupole deformations β_1 and β_2 of nuclei.

Light fragment	β_1	Heavy fragment	β_2	$\hbar\omega_\epsilon$ (keV)	J_ϵ ($\hbar^2$/MeV)	Θ (MeV)
^{100}Sr	0.372	^{152}Nd	0.274	569	58.1	0.84
^{102}Zr	0.421	^{150}Ce	0.274	754	46.1	0.68
^{104}Zr	0.42	^{148}Ce	0.246	799	39.7	0.73
^{104}Mo	0.325	^{148}Ba	0.22	792	34.39	0.82
^{106}Mo	0.353	^{146}Ba	0.218	768	33.13	0.67
^{108}Mo	0.354	^{144}Ba	0.193	779	32.49	0.65
^{112}Ru	0.302	^{140}Xe	0.11	1030	21.28	0.60
^{120}Cd	0.2	^{132}Sn	0.05	1770	6.81	0.10

perdeformed states in actinides [36]. Taking these facts into consideration, we suppose that correct theoretical values of average angular momenta must lie between two lines presented in Figs. 5 and 6 for the standard fission mode. For the splitting Mo+Ba, the calculated average angular momenta of fragments carried by the bending mode are in satisfactory agreement with the experimental data for $\nu<5$. The experimental points are located between two theoretical lines. The theoretical curves correctly describe the functional dependence of data on ν up to $\nu=5$. For the Zr+Ce fragmentation, the experimental points are located below both theoretical curves, but the deviations of theoretical results from the experimental data would not exceed $1.5\hbar$ for $\nu<5$, if we image the theoretical data between two lines presented in Fig. 6.

Comparing the experimental data with results of the calculations, we should note that the angular momenta of pri-

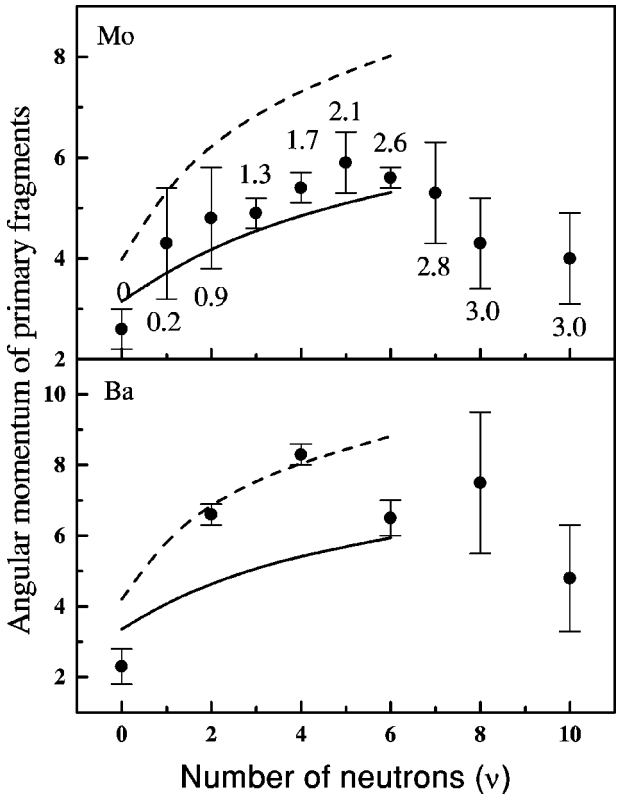

FIG. 5. Calculated and experimental [16] (solid circles) angular momenta (in units of $\hbar$) of fission fragments as a function of the total number of evaporated neutrons ν from both nuclei for the Mo+Ba primary fragmentation of ^{252}Cf. The secondary fragment pairs involve ^{104}Mo with different Ba isotopes. The upper part shows the values for the Mo daughter nuclei; the lower part, those of the corresponding Ba daughter nuclei. The numbers in the upper figure are the adjusted numbers of emitted neutrons from the primary Mo fragments. The calculations for the first fission mode performed with experimental and rigid body moments of inertia are shown by solid and dashed lines, respectively.

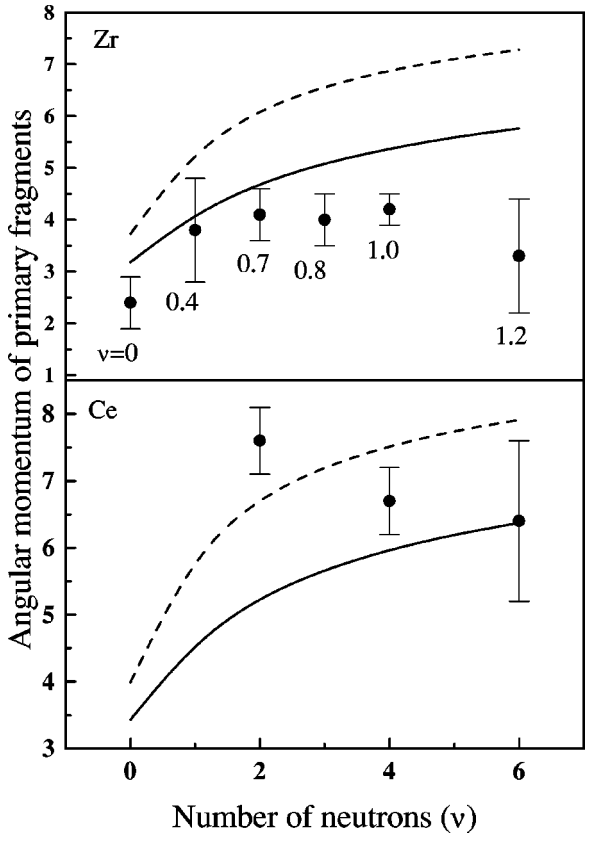

FIG. 6. The same as in Fig. 5, but for the fragmentation of ^{252}Cf into the fragments Zr+Ce. The secondary fragment pairs involve ^{102}Zr with different Ce isotopes.

mary fragments were not directly measured in experiment. From the intensities of the γ transitions between different levels of the spontaneous fission fragment (secondary) the experimentalists determine the level populations and calculate the average angular momentum of the secondary fragment. At this step, the experimental uncertainties (about $2\hbar$) come from the difficulties of subtraction of the background, from the ignorance of exact rotational spectra of spontaneous fission fragments, and from the cases when different isotopes of the same nucleus have the same energy of 2^+ rotational state. To obtain the angular momentum of the primary fragment, the mean number of evaporated neutrons from the fragments and the spin reduction due to the neutron evaporation are calculated within statistical model. This model correction of the angular momenta leads to uncertainties in the experimental results as well. Taking these facts and the discussion in Ref. [35] on the method of extraction of the data from the set of γ transitions into consideration, the agreement of theoretical calculations with the present data is quite satisfactory.

For $\nu > 5$, the calculated values of the angular momenta of the fragments deviate from the experimental ones. Since for $\nu > 5$, the deformation energy ΔB cannot be disregarded in Eq. (18), we overestimate the value of E^* with Eq. (19) and the values of $\langle L \rangle$. Large values of the neutron multiplicity are connected with the second mode of fission that could have a different cluster composition, more complicated than the dinuclear system. Since the interpretation of the second mode, if exists, is not unique, in present paper we did not look for $\langle L \rangle$ at $\nu > 6$.

A correlation between the maxima of yields of fission fragment pairs and of the angular momenta of the fragments is experimentally observed [16,26]. One can assume that the maximal yields of pairs originating from fission events are associated with the minima of the potential energy at the scission point as a function of β_i and of the N/Z ratios in the fragments. The corresponding DNS has the maximal internal excitation energy at the minimum of the potential energy of the fissioning system as compared with the neighboring configurations. As follows from formula (15), the maximal excitation energy leads to a maximal mean angular momentum of the fragments under the same conditions. The value of angular momentum increases with decreasing moment of inertia but not so strongly as with temperature. For example, for the charge splittings (secondary) ^{104}Mo+Ba and ^{102}Zr+Ce of ^{252}Cf, the maxima of yields correspond to $4n$ and to $(2-4)n$ evaporation channels, respectively. So, for these reactions, the angular distributions of fragments as functions of ν have maxima corresponding to the evaporation of $4n$ and $(2-4)n$ neutrons. For the neutronless charge splittings ^{104}Mo+^{148}Ba and ^{102}Zr+^{150}Ce, the values of yields and of mean total angular momenta are smallest as compared to the channels with evaporation of neutrons. In order to describe the yields of fission fragment pairs and of the angular momenta of the fragments simultaneously, one should perform calculations of the multidimensional potential energy surface for the DNS. The latter will allow us to define the DNS temperature in a more correct way.

C. The Coulomb excitation after the DNS decay

In order to calculate the changes of angular momentum of the fragments due to the Coulomb excitation after the DNS decay, we use the following simplified model. The classical Hamiltonian $H_{\rm cl}$ for two flying away fragments P and T is given as

$$H_{\rm cl} = \frac{P_R^2}{2\mu} + + \frac{P_{\theta_P}^2}{2J_P} + \frac{P_{\theta_T}^2}{2J_T} + \frac{Z_P Z_T e^2}{R} + \frac{3}{5}\frac{e^2 Z_P Z_T}{R^3}\sum_{i=T,P} R_i^2 \beta_i Y_2(\theta_i). \quad (21)$$

Since after the DNS decay the distance between the fragments is sufficiently large, one can disregard the interactions between the nuclei in Eq. (21) due to the nuclear forces and higher electric (magnetic) multipole moments. We assume that the interaction between the fragments is dominated by monopole-monopole and monopole-quadrupole terms of Coulomb potential. Angles θ_P, and θ_T describes the orientation of the DNS nuclei with respect to the axis connecting the centers of fragments. P_R, P_{θ_P}, and P_{θ_T} are the canonically conjugated momenta to the coordinates R, θ_P, and θ_T, respectively. In Eq. (21) J_i $(i=T,P)$ is the moments of inertia of the DNS fragments calculated either from the experimental energies of first excited rotational states or from the rigid body approximation.

We consider the relative motion of nuclei starting from $R=R_B=Z_P Z_T e^2/\langle TKE \rangle$ with zero initial velocity (initial kinetic energy $E^0_{\rm kin}=0$). Solving a set of six first order differential equations describing the classical Hamiltonian dynamics for coordinates R, θ_i and momenta P_R, P_{θ_i} $(i=P,T)$, we find the changes of angular momenta $\Delta L_i = \Delta L_i(\theta_P^0, \theta_T^0, L_P^0, L_T^0) = \Delta L_i(\epsilon, L)$ of the DNS fragments as functions of predecay orientation defined by the initial angles θ_P^0 and θ_T^0 and predecay angular momenta L_P^0 and L_T^0. For values of θ_P^0, θ_T^0, L_P^0, and L_T^0 we have $\theta_P^0=\epsilon$, $L_P^0=L$, $\sin|\theta_P^0|/\sin|\theta_T^0| \approx \tilde{R}_T/\tilde{R}_P$ and $|L_P^0 \cos(\theta_P^0)| = |L_T^0 \cos(\theta_T^0)|$. The initial conditions are given by the states of bending mode. The average change of angular momentum for the state with quantum number n of the bending mode is determined as

$$\langle \Delta L_i \rangle_n = \sum_L |b_n^L|^2 \int d\epsilon |\psi_n(\epsilon)|^2 \Delta L_i(\epsilon, L). \quad (22)$$

Since the sign of ΔL_i depends on the initial angular momentum L_i^0, the Coulomb excitation can either increase or decrease the angular momenta of fragments. The average change of angular momentum is calculated as

$$\langle \Delta L_i \rangle = \sum_n P_n \langle \Delta L_i \rangle_n . \quad (23)$$

Before the presentation of numerical results, we give a classical estimate of the Coulomb excitation effect. We will go beyond the sudden approximation taking into consideration the finite moment of inertia of fragments. We assume

TABLE II. Calculated values of the average change of angular momentum $\langle \Delta L_P \rangle_n$ [$\langle \Delta L_P \rangle_n^n$ and $\langle \Delta L_P \rangle_n^a$ are numerical and analytical results using Eq. (26), respectively] of ^{104}Mo nucleus due to the Coulomb excitation for the state with the quantum number n of the bending mode for ^{104}Mo+^{148}Ba split of ^{252}Cf. $\langle L \rangle_n$ is the average angular momentum for the bending state with the quantum number n. The results with the experimental (rigid body) moment of inertia of fragments are on left (right) side of the table.

n	$\langle L \rangle_n$	$\langle \Delta L_P \rangle_n^n$	$\langle \Delta L_P \rangle_n^a$	$\frac{\langle \Delta L_P \rangle_n^n}{\langle L \rangle_n}$	n	$\langle L \rangle_n$	$\langle \Delta L_P \rangle_n^n$	$\langle \Delta L_P \rangle_n^a$	$\frac{\langle \Delta L_P \rangle_n^n}{\langle L \rangle_n}$
0	3.9	1.7	2.0	0.44	0	5.4	1.4	1.6	0.26
1	7.3	1.8	1.9	0.24	1	9.8	1.8	2.0	0.18
2	9.5	1.5	1.6	0.15	2	12.9	1.8	1.9	0.14
3	11.4	1.1	1.1	0.09	3	15.3	1.6	1.8	0.11
4	13.0	0.9	0.8	0.07	4	17.2	1.5	1.5	0.08

that the angle θ_i of rotation approximately changes linearly in time t with frequency L/J_i: $\theta_i(t)=\theta_i^0+Lt/J_i$. This assumption is correct if the change of angular momentum L is small. Solving the equation $\dot{L}_P(t)=-dH_{cl}/d\theta_P$, we obtain the classical change of angular momentum of the fragment P due to the Coulomb excitation

$$\Delta L_P \approx \frac{3}{4} e^2 Z_T Q_P \int_0^\infty dt \frac{\sin\left[2\left(\epsilon+\frac{L}{J_P}t\right)\right]}{R(t)^3}, \qquad (24)$$

where the fragment P with intrinsic quadrupole moment Q_P feels a torque which depends on time t. The angular momentum transferred to rotor is a function of initial orientation ϵ. If the angle of rotation $2Lt/J_i$ remains small during the process considered and $R(t)$ follows the analytical Coulomb trajectory of spherical nuclei [37], the expression (24) can be integrated over time:

$$\Delta L_P \approx \left(\frac{e^2 \mu Z_T}{2Z_P}\right)^{1/2} \frac{Q_P}{R_B^{3/2}} \sin[2\epsilon] + \frac{6\mu Q_P}{5Z_P} \frac{L}{J_P} \cos[2\epsilon]. \qquad (25)$$

Here, the first term is the well-known result of sudden approximation. Taking Eq. (24) and averaging it over the initial conditions which are given by bending state n ($0 \leqslant n \ll \pi/8\gamma_0^2$), we obtain

$$\langle \Delta L_P \rangle_n \approx \frac{3}{4} e^2 Z_T Q_P \cos[2\sqrt{2n+1}\,\gamma_0] \int_0^\infty dt \frac{\sin\left[\frac{2\langle L \rangle_n}{J_P}t\right]}{R(t)^3}. \qquad (26)$$

If $\sin(x) \approx x$, then $\langle \Delta L_P \rangle_n \approx \{6\mu Q_P \cos[2\sqrt{2n+1}\,\gamma_0]/5Z_P\} \times (\langle L \rangle_n / J_P)$ which gives us the evident dependences on n, γ_0, μ, Q_P, Z_P, $\langle L \rangle_n$, and J_P. One can see from calculations that for $n \geqslant 1$, $\langle \Delta L_P \rangle_n$ decreases with increasing n because $\cos[2\sqrt{2n+1}\,\gamma_0]$ decreases faster than $\langle L \rangle_n$ grows. $\langle \Delta L_P \rangle_n$ decreases with increasing moment of inertia J_P. In our approach $\langle \Delta L_P \rangle_n$ does not practically depend on $\langle \mathrm{TKE} \rangle$. We checked by numerical calculations that this dependence is very weak.

The calculated values of $\langle \Delta L_P \rangle_n$ ($n=0-4$) are shown in Table II for the fragmentation ^{104}Mo+^{148}Ba of ^{252}Cf. These analytical results are obtained by using the Eq. (26) and the analytical Coulomb trajectory $R(t)$ for spherical nuclei. Calculations with rigid body and experimental moment of inertia of nuclei give practically the same results. It is seen that $\langle \Delta L_P \rangle_n$ are quite small as compared to the average angular momentum generated by bending vibrations for fission with neutrons evaporation.

VI. SUMMARY

The angular momenta of fission fragments are calculated under the assumption that the bending angular vibrations of DNS are responsible for the generation of angular momenta of the fragments. The calculated results are in qualitative agreement with the experimental data for the ^{252}Cf spontaneous fission. No attempt is made to adjust parameters to fit the experimental data. In contrast to some phenomenological calculations, the angular momenta were not normalized to the experimental value obtained for certain fragments of spontaneous fission. We should stress that the temperature of the system is not a free parameter in our model. It is shown that, for $\nu<5$, the difference Q-TKE mainly corresponds to the excitation energy of internal degrees of freedom of the DNS. This means that the fissioning system is heated before the scission in the case of postscission evaporation of less than five neutrons. The second fission mode of ^{252}Cf, if exists, could deserve complicated cluster interpretation.

ACKNOWLEDGMENTS

We thank Professors W. Greiner, G. M. Ter-Akopian, and V. V. Volkov, Drs. A. V. Daniel, A. K. Nasirov, and G. S. Popeko for fruitful discussions and suggestions. G.G.A. and T.M.S. are grateful for the support of the Alexander von Humboldt-Stiftung and European Physical Society, respectively. This work was supported in part by DFG, RFBR, Volkswagen Stiftung, and STCU (Uzb-45).

APPENDIX: POTENTIAL ENERGY OF DNS AND STIFFNESS OF BENDING MODE

1. Nuclear part of nucleus-nucleus potential

Following the method proposed in Ref. [28], the double-folding procedure is used to calculate the nuclear part of the nucleus-nucleus potential

$$U_N(R,\beta_i,\Omega_i)=\int \rho_1(\mathbf{r}_1)\rho_2(\mathbf{r}_2)F(\mathbf{r}_1-\mathbf{r}_2+\mathbf{R})d\mathbf{r}_1 d\mathbf{r}_2$$
$$=C_0\left[\frac{F_{\rm in}-F_{\rm ex}}{\rho_0}\left(\int \rho_1^2(\mathbf{r})\rho_2(\mathbf{R}+\mathbf{r})d\mathbf{r}+\int \rho_1(\mathbf{r})\rho_2^2(\mathbf{R}+\mathbf{r})d\mathbf{r}\right)+F_{\rm ex}\int \rho_1(\mathbf{r})\rho_2(\mathbf{R}+\mathbf{r})d\mathbf{r}\right]. \quad \text{(A1)}$$

with the effective density-dependent nucleon-nucleon interaction

$$F(\mathbf{r}_1-\mathbf{r}_2+\mathbf{R})=C_0\left[F_{\rm in}\frac{\rho_1(\mathbf{r}_1)+\rho_2(\mathbf{r}_2)}{\rho_0}+F_{\rm ex}\left(1-\frac{\rho_1(\mathbf{r}_1)+\rho_2(\mathbf{r}_2)}{\rho_0}\right)\right]\delta(\mathbf{r}_1-\mathbf{r}_2+\mathbf{R}),$$

$$F_{\rm in,ex}=f_{\rm in,ex}+f'_{\rm in,ex}\frac{N_1-Z_1}{A_1}\frac{N_2-Z_2}{A_2}, \quad \text{(A2)}$$

which is known from the theory of finite Fermi systems [38]. Here, $A=A_1+A_2$ and N_i (Z_i) are neutron (proton) numbers of nuclei. The values of C_0 and the dimensionless parameters $f_{\rm in,ex}$ and $f'_{\rm in,ex}$ are fitted to describe a large number of experimental data [38]. These forces were seriously tested in nuclear structure calculations. For example, the single-particle spectra and characteristics of low-lying collective excitations are well described with these forces (see Ref. [38], and references there). The repulsive core and the pocket in the double-folding nucleus-nucleus potential is obtained naturally when one uses density-dependent nucleon-nucleon interactions. In the pocket of the nucleus-nucleus potential the dinuclear system has the continues shape due to the overlap of diffusion tails of nuclear densities. For the density of deformed nuclei with $A>16$, one can use the two-parameter symmetrized Woods-Saxon function within the intrinsic reference frame of a nucleus ($\mathbf{r}=r,\theta',\phi'$)

$$\rho_i(\mathbf{r},a_i)=\frac{\rho_0\sinh[R_i(\theta',\phi')/a_i]}{\cosh[R_i(\theta',\phi')/a_i]+\cosh(r/a_i)}, \quad \text{(A3)}$$

where $\rho_0=0.17$ fm^{-3} is the density at the center of a nucleus and $a_i=0.55$ fm denotes the diffuseness parameter of an ith nucleus. The shapes of DNS nuclei are described by

$$R_i(\theta',\phi')=R_i\left(1-\frac{\beta_i^2}{4\pi}+\beta_i Y_{20}(\theta',\phi')\right). \quad \text{(A4)}$$

The angles with the prime sign are the angles of $\mathbf{r}$ with respect to the intrinsic coordinate frames of each nucleus. We are interested in the dependence of the DNS potential energy on the orientation angles θ_i with respect to the internuclear axis (molecular frame). Since the functions in Eq. (A1) depend on angles measured in the intrinsic reference frame of each nucleus, we rewrite them with respect to the molecular frame of reference using D functions. The D functions do not depend on integration variables and can be taken out of the integrals [28].

For the analytic calculation of U_N and the reduction of the number of terms in the expansion, we introduce the following modified expansions in the quadrupole deformation parameters β_i for the nuclear density and for the square of the density in the intrinsic coordinate frames:

$$\rho_i(\mathbf{r},a_i)=\rho_i(r,a_i)+\xi\left[R_i\frac{d\rho_i(r,b_i)}{dR_i}\beta_i Y_{20}(\theta',\phi')+\frac{R_i^2}{2}\frac{d^2\rho_i(r,b_i)}{dR_i^2}\beta_i^2 Y_{20}^2(\theta',\phi')\right],$$

$$\rho_i^2(\mathbf{r},a_i)=\rho_i^2(r,a_i)+\xi'\left[R_i\frac{d\rho_i^2(r,b'_i)}{dR_i}\beta_i Y_{20}(\theta',\phi')+\frac{R_i^2}{2}\frac{d^2\rho_i^2(r,b'_i)}{dR_i^2}\beta_i^2 Y_{20}^2(\theta',\phi')\right]. \quad \text{(A5)}$$

The coefficients ξ, ξ', b, and b' in Eq. (A5) are resulted from the fit of the radial dependences of $\rho_i(\mathbf{r},a_i)$ and $\rho_i^2(\mathbf{r},a_i)$ calculated with Eq. (A3) at $\theta'=\alpha_i$ and $\phi'=0$ where the angle α_i corresponds to the nuclear surface point nearest to the other nucleus [28]. Therefore, expression (A5) can be used for any values of β_i and should be considered as an approximation to the correct dependences of $\rho_i(\mathbf{r},a_i)$ and $\rho_i^2(\mathbf{r},a_i)$ on R at fixed θ_i. Note that the terms proportional to β_i^2 in Eq. (A5) were introduced to increase the accuracy of calculations. The assumption of a small overlap of nuclei of the DNS allows us to neglect the dependence of ξ, ξ', b_i, and b'_i on θ' and ϕ' in the calculations of U_N at fixed β_i and θ_i.

Since we are interested in the potential energy under the condition (3), further calculations are performed assuming a small deviation of the ratio between $\tilde{\theta}_1$ and $\tilde{\theta}_2$ from the ratio (3). If the angles $\tilde{\theta}_1=\pi-\theta_1$ and $\tilde{\theta}_2=\theta_2$ are small (small bending vibrations) at $R\approx R_m=\tilde{R}_1+\tilde{R}_2+s$, where $\tilde{R}_i=R_i[1-\beta_i^2/(4\pi)+\sqrt{5/4\pi}\beta_i]$ are the major axes of prolately deformed nuclei, we can use analytic expressions for α_i:

$$\alpha_1=c_{11}\tilde{\theta}_1+c_{12}\tilde{\theta}_2,$$
$$\alpha_2=c_{21}\tilde{\theta}_1+c_{22}\tilde{\theta}_2. \quad \text{(A6)}$$

Here, $c_{11}=1-(\tilde{R}_2+sg_2^2)(g_1^2-1)/(\tilde{R}_1g_2^2+\tilde{R}_2g_1^2+sg_1^2g_2^2)$, $c_{12}=\tilde{R}_2(1-g_2^2)/(\tilde{R}_1g_2^2+\tilde{R}_2g_1^2+sg_1^2g_2^2)$, $c_{21}=\tilde{R}_1(1-g_1^2)/(\tilde{R}_1g_2^2+\tilde{R}_2g_1^2+sg_1^2g_2^2)$, $c_{22}=1-(\tilde{R}_1+sg_1^2)(g_2^2-1)/(\tilde{R}_1g_2^2+\tilde{R}_2g_1^2+sg_1^2g_2^2)$, and $g_i=[1-\beta_i^2/(4\pi)+\sqrt{5/4\pi}\beta_i]/[1-\beta_i^2/(4\pi)-\sqrt{5/(16\pi)}\beta_i]$ is the major-to-minor axis ratio of the ith nucleus.

Inserting the expression

$$\rho_i^2(r,a) = -\rho_0 a \sinh\left(\frac{R_i}{a}\right)\frac{d}{dR_i}\frac{\rho_i(r,a)}{\sinh\left(\frac{R_i}{a}\right)}$$

$$= -\rho_0\left[a\frac{d}{dR_i} - \coth\left(\frac{R_i}{a}\right)\right]\rho_i(r,a)$$

$$= \frac{\rho_0}{F_{in}-F_{ex}}\Lambda_i(a)\rho_i(r,a) \qquad \text{(A7)}$$

into Eq. (A1), using Eqs. (A2), (A5), and taking $\phi_1=\phi_2=0$, the nuclear part of the potential energy is approximately written as

$$U_N(R,\beta_i,\theta_i)$$
$$\approx U_{11}+U_{21}Y_{20}(\theta_2)+U_{22}Y_{20}(\theta_1)+U_{31}Y_{20}^2(\alpha_2)$$
$$+U_{32}Y_{20}(\alpha_1)Y_{20}(\alpha_2)+U_{33}Y_{20}^2(\alpha_1)$$
$$+U_{41}Y_{20}(\alpha_1)Y_{20}^2(\alpha_2)+U_{42}Y_{20}^2(\alpha_1)Y_{20}$$
$$\times(\alpha_2)+U_{51}Y_{20}^2(\alpha_1)Y_{20}^2(\alpha_2), \qquad \text{(A8)}$$

where the coefficients

$$U_{11}=C_0[\Lambda_1(a_1)+\Lambda_2(a_2)+F_{ex}]I_0(a_1,a_2),$$

$$U_{21}=C_0\beta_1R_1\frac{d}{dR_1}[\xi_1\Lambda_2(a_2)I_1(b_1,a_2)$$
$$+\xi_1'\Lambda_1(b_1')I_1(b_1',a_2)+F_{ex}\xi_1I_1(b_1,a_2)],$$

$$U_{22}=C_0\beta_2R_2\frac{d}{dR_2}[\xi_2\Lambda_1(a_1)I_2(a_1,b_2)$$
$$+\xi_2'\Lambda_2(b_2')I_2(a_1,b_2')+F_{ex}\xi_2I_2(a_1,b_2)],$$

$$U_{31}=C_0\beta_2^2\frac{R_2^2}{2}\frac{d^2}{dR_2^2}[\xi_2\Lambda_1(a_1)I_0(a_1,b_2)$$
$$+\xi_2'\Lambda_2(b_2')I_0(a_1,b_2')+F_{ex}\xi_2I_0(a_1,b_2)],$$

$$U_{33}=C_0\beta_1^2\frac{R_1^2}{2}\frac{d^2}{dR_1^2}[\xi_1'\Lambda_1(b_1')I_0(b_1',a_2)$$
$$+\xi_1\Lambda_2(a_2)I_0(b_1,a_2)+F_{ex}\xi_1I_0(b_1,a_2)],$$

$$U_{32}=C_0\beta_1\beta_2R_1R_2\frac{d^2}{dR_1dR_2}[\xi_1'\xi_2\Lambda_1(b_1')I_0(b_1',b_2)$$
$$+\xi_1\xi_2'\Lambda_2(b_2)I_0(b_1,b_2')+\xi_1\xi_2I_0(b_1,b_2)],$$

$$U_{41}=C_0\beta_1\beta_2^2\frac{R_1R_2^2}{2}\frac{d^3}{dR_1dR_2^2}[\xi_1'\xi_2\Lambda_1(b_1')I_0(b_1',b_2)$$
$$+\xi_1\xi_2'\Lambda_2(b_2)I_0(b_1,b_2')+\xi_1\xi_2I_0(b_1,b_2)],$$

$$U_{42}=C_0\beta_1^2\beta_2\frac{R_1^2R_2}{2}\frac{d^3}{dR_1^2dR_2}[\xi_1'\xi_2\Lambda_1(b_1')I_0(b_1',b_2)$$
$$+\xi_1\xi_2'\Lambda_2(b_2)I_0(b_1,b_2')+\xi_1\xi_2I_0(b_1,b_2)],$$

$$U_{51}=C_0\beta_1^2\beta_2^2\frac{R_1^2R_2^2}{4}\frac{d^4}{dR_1^2dR_2^2}[\xi_1'\xi_2\Lambda_1(b_1')I_0(b_1',b_2)$$
$$+\xi_1\xi_2'\Lambda_2(b_2)I_0(b_1,b_2')+\xi_1\xi_2I_0(b_1,b_2)] \qquad \text{(A9)}$$

depend only on the relative distance R and quadrupole deformation parameters β_i. With the Fourier transform of the function $\rho_i(r,a_i)$

$$\rho_i(p,a_i)=\frac{\sqrt{2\pi}a_iR_i\rho_0}{p\sinh(\pi a_ip)}\times\left(\frac{\pi a_i}{R_i}\sin(pR_i)\coth(\pi a_ip)-\cos(pR_i)\right), \qquad \text{(A10)}$$

the following integrals are calculated:

$$I_0(a,b)=-4\pi\int_0^\infty\rho_1(p,a)\rho_2(p,b)j_0(pR)p^2dp,$$

$$I_1(a,b)=-(4\pi)^2\int_0^\infty dpp^2j_2(pR)\rho_2(p,b)\times\int_0^\infty drr^2j_2(pr)\rho_1(r,a),$$

$$I_2(a,b)=-(4\pi)^2\int_0^\infty dpp^2j_2(pR)\rho_1(p,a)\times\int_0^\infty drr^2j_2(pr)\rho_2(r,b). \qquad \text{(A11)}$$

Here, $j_2(pR)$ and $j_0(pR)$ are spherical Bessel functions. Due to the small overlap of DNS nuclei, the spherical functions in some integrands in Eq. (A1) are replaced by their values at $\theta_i'=\alpha_i$ to obtain Eq. (A8). Direct calculations of the corresponding integrals show that this approximation works well [28]. Thus, using Eq. (A6) and expanding the spherical harmonics in small angles $\tilde{\theta}_i$ up to the second order, we obtain

$$U_N=U_{N0}+\frac{1}{2}C_{11}^n\tilde{\theta}_1^2+C_{12}^n\tilde{\theta}_1\tilde{\theta}_2+\frac{1}{2}C_{22}^n\tilde{\theta}_2^2, \qquad \text{(A12)}$$

where

$$U_{N0}=U_{11}+\sqrt{\frac{5}{4\pi}}(U_{21}+U_{22})+\frac{5}{4\pi}\left(U_{31}+U_{32}+U_{33}+\sqrt{\frac{5}{4\pi}}(U_{41}+U_{42})+\frac{5}{4\pi}U_{51}\right),$$

$$C_{11}^{n}=-3\left[\sqrt{\frac{5}{4\pi}}U_{22}+\frac{5}{4\pi}c_{11}^{2}\left(2U_{33}+U_{32}+\sqrt{\frac{5}{4\pi}}(2U_{42}+U_{41})+\frac{5}{2\pi}U_{51}\right)\right.$$
$$\left.+\frac{5}{4\pi}c_{21}^{2}\left(2U_{31}+U_{32}+\sqrt{\frac{5}{4\pi}}(2U_{41}+U_{42})+\frac{5}{2\pi}U_{51}\right)\right],$$

$$C_{12}^{n}=-\frac{15}{4\pi}\left[c_{12}c_{11}\left(2U_{33}+U_{32}++\sqrt{\frac{5}{4\pi}}(2U_{42}+U_{41})+\frac{5}{2\pi}U_{51}\right)\right.$$
$$\left.+c_{21}c_{22}\left(2U_{31}+U_{32}++\sqrt{\frac{5}{4\pi}}(2U_{41}+U_{42})+\frac{5}{2\pi}U_{51}\right)\right],$$

$$C_{22}^{n}=-3\left[\sqrt{\frac{5}{4\pi}}U_{21}+\frac{5}{4\pi}c_{22}^{2}\left(2U_{31}+U_{32}+\sqrt{\frac{5}{4\pi}}(2U_{41}+U_{42})+\frac{5}{2\pi}U_{51}\right)\right.$$
$$\left.+\frac{5}{4\pi}c_{12}^{2}\left(2U_{33}+U_{32}+\sqrt{\frac{5}{4\pi}}(2U_{42}+U_{41})+\frac{5}{2\pi}U_{51}\right)\right]. \tag{A13}$$

2. Coulomb part of nucleus-nucleus potential

For the Coulomb interaction, we use the formula [39]

$$U_C=\frac{Z_1Z_2e^2}{R}+\frac{3}{5}\frac{Z_1Z_2e^2}{R^3}\sum_{i=1}^{2}R_i^2\beta_iY_2(\theta_i)$$
$$+\frac{12}{35}\frac{Z_1Z_2e^2}{R^3}\sum_{i=1}^{2}R_i^2[\beta_iY_2(\theta_i)]^2. \tag{A14}$$

For the small overlap of DNS nuclei, the effect of density diffuseness is relatively small and is neglected in this formula. The expansion of Eq. (A14) in $\tilde{\theta}_i$ $(i=1,2)$ results in

$$U_C=U_{C0}+\frac{1}{2}C_{11}^{c}\tilde{\theta}_1^2+\frac{1}{2}C_{22}^{c}\tilde{\theta}_2^2, \tag{A15}$$

where

$$U_{C0}=\frac{Z_1Z_2e^2}{R}\left\{1+\frac{1}{R^2}\sum_{i=1}^{2}R_{0i}^2\left[\left(\frac{9}{20\pi}\right)^{1/2}\beta_i+\frac{3}{7\pi}\beta_i^2\right]\right\},$$

$$C_{ii}^{c}=-3\frac{Z_1Z_2e^2}{R^3}R_{0i}^2\left[\left(\frac{9}{20\pi}\right)^{1/2}\beta_i+\frac{6}{7\pi}\beta_i^2\right]\quad(i=1,2). \tag{A16}$$

Finally, using Eqs. (A12) and (A15), we obtain the expression for the total potential energy U of DNS in the form of Eq. (1), where $C_{ij}=C_{ij}^{n}+C_{ij}^{c}$.

[1] K. A. Erb and D. A. Bromley, in *Treatise on Heavy-Ion Science*, edited by D. A. Bromley (Plenum, New York, 1985), Vol. 3, p. 201.

[2] K. Wildermuth and Y. Tang, *Unified Theory of Nucleus* (Mir, Moscow, 1980).

[3] W. Greiner, J. Y. Park, and W. Scheid, *Nuclear Molecules* (World Scientific, Singapore, 1995).

[4] V. V. Volkov, *Deep Inelastic Nuclear Reactions* (Energoizdat, Moscow, 1982).

[5] W. U. Schröder and J. R. Huizenga, in *Treatise on Heavy-Ion Science*, edited by D. A. Bromley (Plenum, New York, 1984), Vol. 2, p. 115.

[6] V. V. Volkov, in *Proceedings of the International School-Seminar on Heavy Ion Physics*, Dubna, 1986 (JINR, Dubna, 1987), p. 528; Izv. Akad. Nauk SSSR, Ser. Fiz. **50**, 1879 (1986); in *Proceedings of the International Conference on Nuclear Reaction Mechanisms*, Varenna, 1991, edited by E. Gadioli (Ricerca Scientifica, Milan, 1991), p. 39.

[7] N. V. Antonenko, E. A. Cherepanov, A. K. Nasirov, V. B. Permjakov, and V. V. Volkov, Phys. Rev. C **51**, 2635 (1995); G. G. Adamian, N. V. Antonenko, and W. Scheid, Nucl. Phys. **A618**, 176 (1997); G. G. Adamian, N. V. Antonenko, W. Scheid, and V. V. Volkov, *ibid.* **A627**, 332 (1997); **A633**, 154 (1998); R. V. Jolos, A. K. Nasirov, and A. I. Muminov, Eur. Phys. J. A **4**, 246 (1999); E. A. Cherepanov, Report No. JINR E7-99-99, 1999 (unpublished); G. G. Adamian, N. V. Antonenko, and Yu. M. Tchuvil'sky, Phys. Lett. B **451**, 289 (1999); A. Diaz-Torres, G. G. Adamian, N. V. Antonenko, and W. Scheid, *ibid.* **481**, 228 (2000).

[8] J. R. Nix and W. J. Swiatecki, Nucl. Phys. **A71**, 1 (1965).
[9] J. O. Rasmussen *et al.*, Nucl. Phys. **A136**, 465 (1969).
[10] V. A. Shigin, Sov. J. Nucl. Phys. **3**, 1966 (1966); **14**, 695 (1971).
[11] M. Zielinska-Pfabé and K. Dietrich, Phys. Lett. **49B**, 123 (1974).
[12] B. D. Wilkins, E. P. Steinberg, and R. R. Chasman, Phys. Rev. C **14**, 1832 (1976).
[13] J. O. Rasmussen *et al.*, in *Proceedings of the International Conference on Dynamical Aspects of Nuclear Fission*, Casta-Papiernicka, 1996, edited by J. Kliman and B. Pustylnik (JINR, Dubna, 1996), p. 290.
[14] Yu. V. Piatkov *et al.*, Nucl. Phys. **A611**, 355 (1996); **A624**, 140 (1997).
[15] S. Misicu, A. Sandulescu, and W. Greiner, Mod. Phys. Lett. A **12**, 1343 (1997).
[16] G. S. Popeko *et al.*, in *Proceedings of the International Conference Fission and Properties of Neutron-Rich Nuclei*, 1997, edited by J. H. Hamilton and A. V. Ramayya (World Scientific, Singapore, 1998).
[17] V. V. Volkov, Russ. Atom. Nucl. **59**, 695 (1999).
[18] I. N. Mikhailov and P. Quentin, Phys. Lett. B **462**, 7 (1999).
[19] S. Misicu and P. Quentin, Eur. Phys. J. A **6**, 399 (1999).
[20] S. Misicu *et al.*, Phys. Rev. C **60**, 034613 (1999).
[21] J. Randrup, Nucl. Phys. **A383**, 468 (1982); T. Dossing and J. Randrup, *ibid.* **A433**, 215 (1985).
[22] P. O. Hess and W. Greiner, Nuovo Cimento A **83**, 76 (1984); P. O. Hess, W. Greiner, and W. T. Pinkston, Phys. Rev. Lett. **53**, 1535 (1984).
[23] R. Maass and W. Scheid, Phys. Lett. B **202**, 26 (1988); J. Phys. G **16**, 1359 (1990); **18**, 707 (1992).
[24] E. Uegaki and Y. Abe, Phys. Lett. B **231**, 28 (1989); **340**, 143 (1994); Prog. Theor. Phys. **90**, 615 (1993); Prog. Theor. Phys. Suppl. **132**, 135 (1998).
[25] P. O. Hess, S. Misicu, and W. Greiner, J. Phys. G **26**, 957 (2000).
[26] G. M. Ter-Akopian *et al.*, Phys. Rev. C **55**, 1146 (1997).
[27] P. Fröbrich and R. Lipperheide, *Theory of Nuclear Reactions* (Oxford Science, Oxford, 1996).
[28] G. G. Adamian *et al.*, Int. J. Mod. Phys. E **5**, 191 (1996).
[29] M. Abramowitz and I. A. Stegun, *Handbook of Mathematical Functions* (Dover, New York, 1964).
[30] A. M. Wapstra and G. Audi, Nucl. Phys. **A440**, 327 (1985); S. Liran and N. Zeldes, At. Data Nucl. Data Tables **17**, 431 (1976).
[31] G. G. Adamian, N. V. Antonenko, S. P. Ivanova, and W. Scheid, Nucl. Phys. **A646**, 29 (1999).
[32] S. Raman *et al.*, At. Data Nucl. Data Tables **36**, 1 (1987).
[33] S. Aberg *et al.*, Annu. Rev. Nucl. Part. Sci. **40**, 439 (1990).
[34] R. V. F. Janssens and T. L. Khoo, Annu. Rev. Nucl. Part. Sci. **41**, 321 (1991).
[35] D. C. Biswas *et al.*, Eur. Phys. J. A **7**, 189 (2000).
[36] T. M. Shneidman *et al.*, Nucl. Phys. **A671**, 64 (2000).
[37] K. Adler and A. Winther, *Electromagnetic Excitation* (North Holland, Amsterdam, 1975).
[38] A. B. Migdal, *Theory of Finite Fermi Systems and Application to Atomic Nuclei* (Nauka, Moscow, 1982).
[39] C. Y. Wong, Phys. Rev. Lett. **31**, 766 (1973).